Observations of Phobos by the Mars Express radar MARSIS: Description of the detection techniques and preliminary results

A. Cicchetti[1,*], C. Nenna[2], J.J. Plaut[3], D. Plettemeier[4], R. Noschese[1], M. Cartacci[1], R. Orosei[5]

[1] Istituto di Astrofisica e Planetologia Spaziali (IAPS), Istituto Nazionale di Astrofisica (INAF), Rome, Italy.

[2] Info Solution, Milan, Italy.

[3] Jet Propulsion Laboratory, Pasadena, CA, USA.

[4] University of Dresden, Radio Frequency and Photonics, Dresden, Germany.

[5] Istituto di Radioastronomia, Istituto Nazionale di Astrofisica, Bologna, Italy.

panic@mediacom.it (Carlo Nenna, Milan, Italy)

jeffrey.j.plaut@jpl.nasa.gov (Jeffrey J. Plaut, Pasadena, California)

dirk.plettemeier@tu-dresden.de (Dirk Plettemeier, Dresden, Germany)

raffaella.noschese@iaps.inaf.it (Raffaella Noschese, Rome, Italy)

marco.cartacci@iaps.inaf.it (Marco Cartacci, Rome, Italy)

roberto.orosei@inaf.it (Roberto Orosei, Bologna, Italy)

Keywords: Phobos; Mars; Radar; Mars Express ESA mission; MARSIS; Ground penetrating radar.

* Corresponding author:

Andrea Cicchetti

Email addresses: andrea.cicchetti@iaps.inaf.it

Phone: +390645488750

Fax: +39 06 4993 4383

ABSTRACT

The Mars Advanced Radar for Subsurface and Ionosphere Sounding (MARSIS) (Picardi et al., 2005) is a synthetic aperture low frequency radar altimeter, onboard the ESA Mars Express orbiter, launched in June 2003. It is the first and so far the only spaceborne radar that has observed the Martian moon Phobos. Radar echoes were collected on different flyby trajectories. The primary aim of sounding Phobos is to prove the feasibility of deep sounding, into its subsurface.

MARSIS is optimized for deep penetration investigations and is capable of transmitting at four different bands between 1.3 MHz and 5.5 MHz with a 1 MHz bandwidth. Unfortunately the instrument was originally designed to operate exclusively on Mars, assuming that Phobos would not be observed. Following this assumption, a protection mechanism was implemented in the hardware (HW) to maintain a minimum time separation between transmission and reception phases of the radar. This limitation does not have any impact on Mars observation but it prevented the observation of Phobos.

In order to successfully operate the instrument at Phobos, a particular configuration of the MARSIS onboard software (SW) parameters, called "Range Ambiguity," was implemented to override the HW protection zone, ensuring at the same time a high level of safety of the instrument.

This paper describes the principles of MARSIS onboard processing, and the procedure through which the parameters of the processing software were tuned to observe targets below the minimum distance allowed by hardware.

Some preliminary results of data analysis will be shown, with the support of radar echo simulations. A qualitative comparison between the simulated results and the actual data, does not support the detection of subsurface reflectors.

1. Introduction

Mars Express, the first European interplanetary mission, was designed to provide global coverage of Mars' surface, subsurface, atmosphere and to study the Martian moons, Phobos and Deimos (Chicarro et al., 2004). The Mars Advanced Radar for Subsurface and Ionosphere Sounding (MARSIS) is one of the seven scientific instruments onboard of Mars Express orbiter. Its primary goal is to search for water, both solid and liquid, in the subsurface of Mars. MARSIS, in order to penetrate the surface and detect dielectric discontinuities, due to subsurface layers, transmits radio signals characterized by low frequencies and wide band (Picardi et al., 2004).

With the aim to achieve these ambitious scientific goals and in order to cope with some limitation imposed by the mission characteristics, such as the limited data-rate provided by the spacecraft and the limited available downlink data volume, it was necessary to design an instrument with high computational capabilities.

For these reasons, the onboard software is characterized by a high grade of flexibility that allows the possibility to modify the signal processing in order to face unpredictable issues arising during the mission. This capability was very useful when, after several years of Mars observation, Phobos became a scientific objective for MARSIS too (Cicchetti et al., 2011).

Phobos is a non-spherical body with a mean radius of 11 km, and its quasi circular orbit is located on the equatorial plane of Mars. The distance from Phobos to the center of Mars is about 9378 km while the orbital period is 7,65 hours.

The origin of Phobos, in spite of 45 years of spacecraft observations, is still debated (Duxbury et al., 2014). The two main hypotheses on the origin of this moon are in situ formation and

asteroidal capture. Considering size, shape and past estimations of composition (Burns, 1978; Forget et al., 2008; Murchie et al., 1991), the the theory of the asteroidal capture origin was favored by the majority of researchers. However, more recent studies (Andert et al., 2010; Giuranna et al., 2011; Pätzold et al., 2014; Rosenblatt et al., 2010; Witasse et al., 2014) support the conclusion that the composition and bulk density are more consistent with the in situ formation scenario. Thus, the moon is likely to have formed from a disk of impact ejecta produced by a giant collision early in Mars history.

The Martian moon could be observed during several close flybys, thanks to the high eccentricity of the Mars Express orbit (Witasse et al., 2014). The first observation executed with the MARSIS radar, was taken on November 4th 2005 (orbit 2323) . The shortest distance between the radar antenna and the Phobos surface was only 215 km, that allowed to obtain a good signal to noise ratio (SNR) of ~25 dB after the on ground data processing. Subsequent flybys allowed observations even within 100 km of the surface (Safaeinili et al., 2009).

In many Phobos flybys observed by the radar so far, we have been able to identify several interesting secondary echoes, that could be generated either by surface lateral clutter or by sub-subsurface reflectors.

In order to discriminate between the two possible origins of detected echoes, an incoherent surface backscattering simulator (Russo et al., 2008) was used.

The simulations, which try to reproduce the radar signal backscattering, use the digital elevation model made available by the High Resolution Stereo Camera (HRSC) science team (Willner et al., 2013), and were computed for one of the closest flybys.

2. Mars observation fundamentals

A typical MARSIS observation of Mars consists of a sequence of synthetic apertures (frames), a Frame being a set of Pulse Repetition Intervals (PRIs) as shown in Fig. 1 and Fig. 2.

Each MARSIS observation Frame is made of the following sequence of operations performed onboard:

- Initial orbital parameter estimation, including Frame size estimation (NB, number of PRIs).
- Synthetic aperture size estimation (NA_1 PRIs for the first band, NA_2 PRIs for the second band).
- Signal transmission (2 pulses) and echo reception, repeated NA_1 times and NA_2 times.
- Signal Processing for both the bands.

The frame size NB is computed adaptively during the flyby in order to obtain contiguous synthetic apertures, so that their relative separation precisely matches with the distance covered by the spacecraft, in the time elapsed between the two apertures. This guarantees the continuous coverage along the orbit track.

The space to be covered by the spacecraft during NB pulses, related to a single frame, is computed first as:

$$\Delta S = \sqrt{\frac{\lambda_1 \cdot H}{2}} + N_o \cdot \frac{V_{Tan}}{PRF} \qquad (1)$$

where **PRF** is the Pulse Repetition Frequency (1/PRI = 127.267 Hz), $\mathbf{N_o}$ is a constant offset of 36 PRIs, $\boldsymbol{\lambda_1}$ is the wavelength of the lowest Operative Frequency in use (available center frequencies are 5Mhz, 4MHz, 3MHz and 1.8MHz), **H** and $\mathbf{V_{Tan}}$ **are the spacecraft altitude and the tangential velocity respectively.**

Frame size NB is then computed as :

$$NB = Int\left[\frac{\Delta S}{V_{Tan}} \cdot PRF\right] \quad (2)$$

Synthetic aperture sizes $\mathbf{NA_1}$ and $\mathbf{NA_2}$ are also adaptively computed for each of the operative frequencies in use:

$$NA_1 = Int\left[\lambda_1 \cdot \frac{H \cdot PRF}{2 \cdot \gamma_1 \cdot V_{Tan} \cdot \Delta S}\right] \quad (3)$$

$$NA_2 = Int\left[\lambda_2 \cdot \frac{H \cdot PRF}{2 \cdot \gamma_2 \cdot V_{Tan} \cdot \Delta S}\right] \quad (4)$$

Where $\boldsymbol{\gamma_1}$ and $\boldsymbol{\gamma_2}$ are corrective frequency dependent values, necessary to obtain the same azimuth resolution in different bandwidths.

A single PRI operation, repeated NA times (NA = max(NA_1, NA_2)), will then include signal transmission and echo reception, according to the scheme shown in Fig. 3.

MARSIS transmits two rectangular pulses, each one 250 μs long, modulated in frequency (chirp) with a 1 MHz bandwidth centered on the selected operative frequency. **In this way the radar free-space range resolution is approximately 150m (Cook and Bernfeld, 1967, eq. 1-19), which**

corresponds to 50-100 m in the subsurface, depending on the real dielectric constant of the subsurface. The time delay between the two transmitted pulses is fixed at 450 μs, while the *Trigger* values for receive (RX) gate positioning are adaptively computed for each frame taking into account the spacecraft height and the ionosphere effect **(Safaeinili et al., 2003)**, which introduces a delay that can be from 50 up to 150 μs. The first frame (*Frame 1*) *Trigger* values are computed with the following equation:

$$Trigger = \frac{2 \cdot H}{c}\left[\mu s\right] + \Delta t \qquad (5)$$

where $\boldsymbol{c}$ is the speed of light in the free space, **H** is the spacecraft altitude and $\Delta\mathbf{t}$ is a preset offset added to compensate for the ionosphere delay. For the subsequent frames (*Frame n*, $n > 1$) *trigger* values are estimated using the results of the surface echo tracking processing executed on the preceding frame (*Frame n-1*).

During each synthetic aperture NA_1/NA_2 PRI's received echoes are processed by MARSIS in order to synthesize three Doppler filters. The geometric configuration of the doppler filters is obtained using a different phase factor in order to observe different areas on the surface. In particular the Doppler Filter 0 (in the along track direction) is nadir pointing, while the Doppler Filter -1 is looking ahead and the Doppler Filter +1 is looking behind.

Range compression processing is then executed by MARSIS on the central Doppler filter data, followed by surface echo tracking. As previously stated, surface echo tracking results are used to fine tune echo reception in the subsequent frame, taking into account the surface echo delay measured in the current frame.

This common way of operating the instrument, called "subsurface sounding," allows us to observe Mars continuously for up to ~30 minutes (a ground track ~1200 km long), without overloading the spacecraft resources in terms of data rate and data volume capabilities. **An example of the resulting radargram is shown for Band 2 (3MHz) and Band 3 (4MHz) in Fig. 4, representing a typical MARSIS observation over Olympus Mons acquired in orbit 6051. The surface trace follows the profile expected from MOLA topography.**

Subsurface sounding is usually performed when the spacecraft altitude relative to Mars is between 900 km and 240 km. In particular, the lower limit of 240 km altitude, which is lower than the typical Mars Express orbit pericenter altitude, is also a physical limitation implemented in MARSIS instrument as the lowest *trigger* value programmable for the RX gate positioning, as shown in Fig. 3.

The subsurface sounding operative mode we initially designed was therefore optimized for Mars observation, but it was not suitable for Phobos, as the most favorable observation condition for Phobos is typically when spacecraft range to Phobos is less than 240 km, due to the small dimension of the target.

3. System Constraints and Science Requirements

Due to Phobos' small dimensions, it is not possible to take advantage of the onboard processing capabilities of the instrument. That is the nominal subsurface sounding onboard processing, applied to Phobos would provide unreliable results, both for science (results of the Doppler processing) and echo signal tracking (capability of optimizing the surface echo reception). Moreover, as explained before, a physical design limitation precludes MARSIS operation, when the target range is less than 240 km.

In order to successfully observe Phobos at a distance closer than 240 km we therefore decided to apply the following strategy:

- Disable the automatic tracking capability of the onboard software, relying only on the predicted observation geometry parameters.

- Use the same frequency for the two transmitted pulses and manipulate the observation by injecting a range offset of 450μs, in order to reduce the observation altitude limitation from 240 km down to ~ 180 km.

- Make use of a dedicated storage called Flash Memory (FM) that allows us to store a limited but still significant amount of continuous raw unprocessed data, that once transmitted to the ground can be processed with dedicated algorithms.

The removal of the tracking phase is not an issue for Phobos observations. Indeed, the main task of the tracking is to remove the extra time delay introduced by the Martian ionosphere from the radar signal. The absence of this constraint for Phobos allows the evaluation of the trigger value for the reception of surface echoes, considering only the predicted spacecraft range and the speed of light in free space.

The various processing phases also need to be modified, since they are designed to achieve the best performance in the case of Mars observation. In particular, we decided to collect a single synthetic aperture ("super frame"), instead of a number of short frames separated by gaps that would be less useful for science analysis (see Fig. 5).

For this aim, we condition the onboard frame size estimation, enlarging the $\boldsymbol{N_o}$ parameter value in Eq. (1), so that a pair of super frames will be executed during the observation. These settings, together with the capability to send to the ground the raw radar signals using the FM feature, allow us to process the data in an optimal way.

Due to the small dimensions and the irregular shape of Phobos, the possibility of reducing the minimum altitude of the observations is important in order to improve the SNR of the received signals. **Considering the well-known equation of the Signal To Noise Ratio (SNR) (Skolnik, 1990, eq. 1.1-1.4):**

$$SNR = \frac{P_t G_t^{\,2} \lambda^2 \sigma}{(4\pi)^3 H^4 k T_s B} \tag{6}$$

Where P_t is the transmitted power, G_t the antenna gain, λ the wavelength, σ the radar cross section, H the spacecraft altitude, k the Boltzmann's constant, T_s the system noise temperature and B the receiver bandwidth. The theoretical improvement of the SNR, due to a reduction of the operative altitude, is given by the following relation:

$$\Delta_{SNR}\big|_{\mathrm{dB}} = 40 \cdot \log_{10}\left(\frac{H_1}{H_2}\right) \tag{7}$$

Where H_1 is the minimum S/C altitude allowed by the instrument protection mechanism and H_2 is the reduced altitude achieved injecting a range offset of 450μs. Considering H_1=240 km and H_2= 180 km, the improvement of the SNR is ~5dB. This achievement is obtained through the so called "range ambiguity" technique (see Fig. 6), that consists in the evaluation of the trigger offset as follows:

$$Trigger = \frac{2 \cdot H_{amb}}{c} [\mu s] - \Delta t \tag{8}$$

where H_{amb} represents the spacecraft height with an offset of 450μs ($H_{amb} = H + 450\mu s$) and the value of Δt is a margin that takes into account the potential inaccuracy of predicted spacecraft range to Phobos.

Adding this offset we force the instrument to receive the echo of the second transmitted pulse ("echo F2" in Fig. 6) into the first receiving window (Rx_1_F1). The echo of the first transmitted pulse ("echo F1" in Fig. 6) is therefore lost and the second receiving window (Rx_2_F2) will sample just cosmic noise. **For this reason it is necessary to set the same frequency for both transmitted bands, so that the receiver of the first receiving window is correctly configured for the signal detection.** Thanks to the range ambiguity technique we can reduce the observation altitude limitation, from 240 km down to ~ 180 km, thus improving the SNR.

The planning of a single super frame requires careful evaluation of the preset value for the trigger, as this will remain fixed for the overall duration of the flyby.

4. Data Acquisition Strategy

MARSIS is equipped with **16.77MByte** of Flash Memory device dedicated to raw data storage.

The use of this feature is affected by some design constraints:

- raw data received during a single frame are initially stored in a temporary buffer
- stored data need then to be entirely moved from the temporary buffer to non-volatile memory before new data can be acquired.

Due to the intrinsic data write latency of FM device, raw data need to be first stored into temporary RAM buffers (one for each received channel). Each RAM buffer can store up to 3.21 MByte of data. The time required for data transfer and storage into FM is ~7.0μs per byte. While data transfer to FM is in progress no raw data acquisition to RAM buffers may be executed. Given these constraints the following considerations apply when we design a Phobos observation:

- For each PRI a single received echo, after A/D conversion, consists of 980 8 bit samples. The maximum number of consecutive echoes we can acquire is therefore given by the following equation:

$$N_{Echoes=} \frac{Buffer_{Dimension} - Header_{Dimension}\,[Byte]}{Echo_{Dimension}\,[Byte]} \approx 3270 \qquad (9)$$

Where the Header is a packet of ancillary data, automatically inserted by the onboard SW in order to identify the echoes stored into the FM.

- Keeping a margin of 70 PRI, the maximum synthetic aperture size (NA) of a super frame is equal to 3200 PRI per radar channel.

- The time necessary to transfer 6400 PRI (3200 PRI per channels) from RAM buffers into FM devices is given by the following equation:

$$readout_{Time} = 6400[PRI] \cdot 980[samples] \cdot 1[byte] \cdot 7 \cdot 10^{-6} \approx 44\text{sec} \quad (10)$$

- Considering the Pulse Repetition Frequency (PRF) of 127.267[Hz] the duration of each "super frame" is given by the following equation:

$$Superframe_{Duration} = \frac{1}{PRF} \cdot 3200[PRI] \approx 25.14\text{sec} \quad (11)$$

- Given the total capacity of FM device, the maximum number of Super Frames we can acquire in a single Phobos observation is given by the following equation:

$$N_{SuperFrames} = \frac{Flash_{MemoryDimension}[Byte]}{3200[PRI] \cdot 2[channels] \cdot 980[samples] \cdot 1[byte]} \approx 2.6 \quad (12)$$

In order to maximize the quality of the acquired data, taking into account all of the above considerations and depending on:

– the spacecraft altitude at closest approach
– the spacecraft radial velocity near closest approach

we apply one of the three following strategies:

1) One super frames, centered on closest approach. This is typically used when the closest approach altitude is higher than 180 km, as shown in Fig. 7

2) Two super frames, symmetric with respect to pericenter. This is typically used when the closest approach altitude is lower than 180 km and the spacecraft is at an altitude lower than 180 km for more than 25 seconds, as shown in Fig. 8

3) Three super frames, where the first and third super frame are symmetric to pericenter, while the second super frame is centered on closest approach, as shown in Fig. 9. This is typically used when the closest approach altitude is higher than 180 km and the space craft altitude, within the first and third super frame is below 350 km, as that is the maximum space craft altitude to detect Phobos with a reasonable SNR.

In the following, results obtained applying the "Two Super Frames Technique" and the "Three Super Frames Technique" will be presented, and data collected in two representative Phobos flybys will be discussed.

5. Application of Two Super Frames Technique (Phobos flyby 26 August 2015, orbit 14776)

This flyby took Mars Express very close to Phobos with a minimum approach distance of only 51 km from the surface of the Martian moon. The most appropriate observation strategy for this scenario utilized two super frames, symmetric with respect to the closest approach.

Fig. 10 shows the simulation over about 4.5 minutes around closest approach. The red area represents the instrument protection zone, where it is not possible to operate. The thin blue and red curves represent the ideal receiving window boundaries for acquiring the two echoes reflected by Phobos' surface from the two chirp waves transmitted by the radar. These ideal values vary following the Phobos range profile. The marked blue and red lines represent the real boundaries we programmed for receiving the two echoes. They are constant values, as it's not possible to make use of the automatic echo tracking feature of MARSIS when we observe Phobos.

Once the receiving windows boundaries were determined, we had to calculate the exact timing of the two super frames, before and after the closest approach. From T3 to T4 (approach super frame) and from T7 to T8 (departure super frame) it is possible to collect up to 696 full echoes, however considering that the optimal size for a single super frame is 3200 echoes we collected an additional 2503 reduced echoes per super frame. The best solution was therefore to enable the first super frame at time T2 (2503/2 PRI before T3) and to enable the second super frame at time T6 (2503/2 before T7). Due to some inaccuracy of the predicted orbital parameters we obtained a slightly different distribution of the data in the actual observation, as shown in Fig. 11 and in Fig. 12

The ground processing results of the collected data are presented in Fig. 13 and Fig. 14, for the approach and departure super frame, respectively.

In the top panels of Fig. 13 and Fig. 14 the raw signals have been first compressed in range, with the ideal chirp and then in azimuth in order to improve the SNR. The azimuth compression consists of summing groups of echoes (10 range compressed echoes) after compensating the linear phase term of the received signals. The dark red traces (a, b, c, d and e) of Fig. 13 and Fig.14 represent the echoes reflected by the Phobos' surface. The slopes of the traces are due to the distance from Phobos' surface to the radar, that gradually decreases over time for the approach super frame and gradually increase for the departure super frame. The trace (a) of Fig. 13 is due to the tails of the echoes generated by the first transmission phase and received in the first receiving window, as also highlighted by the dotted rectangle "A" of Fig. 11. None of the signals of Fig. 13 and Fig. 14 have been voluntarily realigned, without compensating the effect of Phobos to spacecraft range variation over time, to provide a more realistic acquisition scenario to the reader.

The presence of separate tracks, "b" and "c" of Fig. 13 and "d" and "e" of Fig. 14 are a side effect of the discrete Fourier transform, which focuses the signal's energy, initially spread over 250 μs, into a single μs at the beginning of the signal itself. Feeding the discrete Fourier transform with a signal truncated of its initial part (X μs truncation at the beginning of the signal), as happens after time T4 in Fig. 11 and before time T7 of Fig. 12, produces a shift in time domain compressed signal equal to 350-X μs.

The bottom panels of Fig. 13 and Fig. 14 show the SNR behavior. The departure super frame (Fig. 14) presents a signal to noise ratio (SNR) with a maximum value of 25 dB, while the approach super frame (Fig.13) presents a maximum value of just 15 dB; this difference of about 10 dB is probably because of a more favorable radar environment in the departure super frame, like flatter surfaces and surfaces more perpendicular to the radar propagation signals.

The data acquired continuously, during the spacecraft movement, are typically presented in the form of radargrams, realigned with the target (Phobos) topography and shown in Fig. 15, in which the horizontal dimension is the frame number, the vertical one is the round trip time of the echo, and the brightness of the pixel is a function of the strength of the echo.

6. Application of Three Super Frames Technique (Phobos flyby 22 February-2013, orbit 11634)

This flyby took Mars Express to a minimum distance of 185 km from the surface of Phobos; therefore the most appropriate timeline was deemed to be the three super frames technique, as described in paragraph 4 and Fig.9.

The approach super frame started at 2013-02-22T11:51:09.483 and consisted of 2665 PRI; the closest-approach super frame started at 2013-02-22T11:52:12.500 and consisted of 3200 PRI, while the departure super frame started on 2013-02-22T11:53:22.518 and consisted of 2673 PRI. The technique adopted for determining the onboard configuration parameters is identical to the one described in paragraph 5.

Data are analyzed for the closest-approach super frame only, as shown in Fig.16. In the other two super frames, data quality was too poor, probably due to surface geometry, which was unfavorable to radar detection.

The received signals from Phobos contain not only echoes from the sub-spacecraft portion of the surface, but also secondary reflections; these latter could be produced by the presence of dielectric discontinuities in the subsurface (i.e. subsurface layers). Surface contributions are expected at the beginning of the echo, while additional signatures, like subsurface reflections, should appear later in the echo. However, depending on surface morphology, surface contributions could produce also secondary reflections. This may occur in case of surface lateral clutter, that can be easily mistaken for subsurface features.

In order to clearly identify the source of all the signatures visible in the radargram, a radar signal simulator of Phobos surface scattering based on the one produced for Mars by (Russo et al., 2008) and using the Phobos Digital Elevation Model (Willner et al., 2013).

The very high quality of echoes collected in this flyby is clearly visible in the upper panel of Fig.16, showing three strong signatures of radar interactions with Phobos.

The lower panel of Fig.16 shows the results of the incoherent simulations of radar returns. Since the three signatures are present both in the real and in the simulated data, we conclude that the presence of subsurface reflectors is unlikely.

Fig. 17 shows the signal behavior for one frame (frame 227, dotted lines in Fig.16). The continuous line represents the actual echo, while the dotted line represents the simulated one. The two profiles do not perfectly overlap, presumably because of approximations in the Phobos shape model.

7. Conclusion

In this paper we have described the theoretical and technical efforts developed to allow a radar sounder designed to probe Mars to also collect high quality data from a completely different target such as Phobos. Thanks to the flexible design of the MARSIS onboard SW and architecture, it has been possible to achieve this goal.

The development of the "range ambiguity" technique allowed to overcome instrument constraints and to collect valuable data, well below the original lowest operative altitude and with an increased SNR.

In spite of the complexity of the required radar settings and the challenging geometric conditions, the experiment was a complete success; and for the first time a radar transmitting a signal of decameter wavelengths observed Phobos, collecting data of high scientific interest.

A preliminary comparison (Fig.16) between simulated and actual signals provides no evidence of subsurface reflectors, while secondary echoes seem to be due to surface clutter. However, a more in-depth study of the signals collected in fifteen flybys is ongoing, because of their potential relevance for future space missions carrying radar sounders and for the understanding of Phobos' formation processes.

Future activities in the analysis of MARSIS data acquired at Phobos will include:

1) performing an advanced comparison with simulated data obtained through a more accurate surface backscattering simulator, based on physical optics and the method of moments (Plettemeier et al., 2009).

2) investigating the capability to obtain information about the composition and the internal structure of Phobos starting from the signal shape and power and if detected, from subsurface reflectors.

Acknowledgement

The authors acknowledge the support of the space agencies of Italy (ASI) and the United States (NASA), for the development and science operations of MARSIS. Operations of the Mars Express spacecraft by the European Space Agency (ESA) are gratefully acknowledged. A special thank you goes to our colleague and friend Ali Safaeinili who passed away last in July 2009. He was one of the great pioneers in the observation of Phobos and one of the most active scientists of the MARSIS radar team.

With fond memories of Professor Giovanni Picardi, conceiver of the MARSIS instrument, our leader and friend, who passed away last in August 2015.

This work was supported by the Italian Space Agency (ASI) through contract no. I/032/12/1.

References

Andert, T.P. et al., 2010. Precise mass determination and the nature of Phobos. Geophys. Res. Lett. 37, L09202.

Burns, J.A., 1978. On the orbital evolution and origin of the martian moons. Vistas Astron. 22, 193–210.

Chicarro, A., Martin, P., Trautner, R., 2004. The Mars Express mission: an overview. In: Wilson, A., Chicarro, A. (Eds.), Mars Express: The Scientific Payload vol. 1240. ESA Special Publication, Noordwijk, The Netherlands, pp.3-13.

Cicchetti, A., and 12 colleagues 2011. MARSIS: Latest Phobos Flyby. Data Processing Results and Advanced Radar Configuration Design. EPSC-DPS Joint Meeting 2011 497.

Cook C.E., Bernfeld M., Radar Signals, Academic Press, New York, 1967

Duxbury, T.C. et al., 2014. Spacecraft exploration of Phobos and Deimos. Planet. Space Sci. 102, 9.

Forget, F., Costard, F., Lognonné, P., 2008. Planet Mars: Story of Another World. Praxis Publishing, Chichester.

Giuranna, M. et al., 2011. Compositional interpretation of PFS/MEx and TES/MGS thermal infrared spectra of Phobos. Planet. Space Sci. 59 (1), 1308–1325.

Murchie, S.L. et al., 1991. Color heterogeneity of the surface of PHOBOS – Relationships to geologic features and comparison to meteorite analogs. J. Geophys. Res. 96, 5925–5945, ISSN 0148-0227.

Pätzold, M. et al., 2014. Phobos: Observed bulk properties. Planet. Space Sci. 102, 86–94.

Picardi, G., Biccari, D., Seu, R., Marinangeli, L., Johnson, W. T. K., Jordan, R. L., Plaut, J., Safaenili, A., Gurnett, D. A., Ori, G. G., Orosei, R., Calabrese, D., Zampolini, E., 2004. Performance and surface scattering models for the Mars Advanced Radar for Subsurface and Ionosphere Sounding (MARSIS). Planet. Space Sci. 52, 149-156.

Picardi G., Plaut J. J., Biccari D., Bombaci O., Calabrese D., Cartacci M., et al., 2005: Radar Soundings of the Subsurface of Mars, Science, Vol. 310, pp. 1925-1928.

Plettemeier, D., Hahnel, R., Hegler, S., Safaeinili, A., Orosei, R., Cicchetti, A., Plaut, J., Picardi, G. 2009. Simulation of Radar-Backscattering from Phobos - A Contribution to the Experiment MARSIS aboard MarsExpress. EGU General Assembly Conference Abstracts 11, 3763.

Rosenblatt, P., et al., 2010. Revisiting Phobos’ origin issure from Mars Express Radio- Science observations. EPSC Abstracts, 1–2.

Russo, F., and 8 colleagues 2008. An incoherent simulator for the SHARAD experiment. Radar Conference, 2008. RADAR '08. IEEE 26-30 May 2008, 1.

Safaeinili, A., W. Kofman, J.-F. Nouvel, A. Herique, and R. L. Jordan (2003), Impact of Mars ionosphere on orbital radar sounder operation and data processing, Planetary and Space Science, 51, 505-515, doi:10.1016/S0032-0633(03)00048-5.

Safaeinili, A., Cicchetti, A., Nenna, C., Calabrese, D., Plettemeier, D., Orosei, R., Duxbury, T., Plaut, J.J., Picardi, G., Flamini, E. 2009. Radar Sounder Observations of Phobos. European Planetary Science Congress 2009 717.

Skolnik, Merrill I., Radar Handbook, Mc Graw Hill, New York, 1990

Willner, K., Shi, X., Oberst, J. 2013. Phobos' shape and topography models. Planetary and Space Science 102 (2014) 51–59.

Witasse, O., and 41 colleagues 2014. Mars Express investigations of Phobos and Deimos. Planetary and Space Science 102, 18-34.

Figure Captions

Fig. 1 Sequence of Frames in a typical observation of Mars, a frame being a set of Pulse Repetition Intervals (PRIs)

Fig. 2 Internal structure of a generic MARSIS frame

Fig. 3 Single PRI operation, repeated NA times. It includes signal transmission and echo reception.

Fig. 4 MARSIS typical acquisition data from orbit 6051, showing a typical observation over Olympus Mons.

Fig. 5 Top panel shows frames separated by gaps to achieve the best performance on Mars. Bottom panel shows a single synthetic aperture ("Super Frame") more appropriate for the observation and science analysis of Phobos.

Fig. 6 Scheme of acquisition with the "Range Ambiguity Technique". The instrument is forced to receive the echo of the second transmitted pulse (“echo F2”) into the first receiving window (Rx_1_F1). The echo of the first transmitted pulse (“echo F1”) is therefore lost and the second receiving window (Rx_2_F2) will sample just cosmic noise.

Fig. 7 Acquisition architecture of single super frame, centered on closest approach. This is typically used when the closest approach altitude is higher than 180 km.

Fig. 8 Acquisition architecture of two super frames symmetric with respect to pericenter. This is typically used when the closest approach altitude is lower than 180 km and the spacecraft is at an altitude lower than 180 km for more than 25 seconds.

Fig. 9 Acquisition architecture of three super frames, centered on closest approach. This is typically used when the closest approach altitude is higher than 180 km and the space craft altitude, within the first and third super frame is below 350 km.

Fig. 10 Simulation over about 4.5 minutes around closest approach. The red area represents the instrument protection zone. The thin blue and red curves represent the ideal receiving windows boundaries for acquiring the two echoes reflected by Phobos' surface from the two chirp waves transmitted by the radar. These ideal values vary following the Phobos range profile. The marked blue and red lines represent the real boundaries programmed for receiving the two echoes.

Fig. 11 Approach Super Frame, actual signal distribution. Due to some inaccuracy of the predicted orbital parameters, we obtained a slightly different distribution of the data.

Fig. 12 Departure Super Frame, actual signal distribution. Due to some inaccuracy of the predicted orbital parameters we obtained a slightly different distribution of the data.

Fig. 13 Phobos science results of the approach super frame. The top panel shows the range and azimuth compression processing. The bottom panel shows the signal to noise ratio(SNR) behavior. The traces "a", "b" and "c" represent the echoes reflected by the Phobos surface.

Fig. 14 Phobos science results of the departure super frame. The top panel shows the range and azimuth compression processing. The bottom panel shows the signal to noise ratio(SNR) behavior. The traces "d" and "e" represent the echoes reflected by the Phobos surface.

Fig. 15 Phobos radargram of orbit 1476 re aligned with the surface topography. The top panel shows the approach super frame, while the bottom panel shows the departure super frame.

Fig. 16 Phobos radargram of the closest Super Frame. The top panel shows the range and azimuth compression processing of the real data, while the lower panel shows the incoherent simulation of the radar surface returns.

Fig. 17 Frame 227 behavior. The continuous line represents the actual processed data while the dotted line represents the simulated data.

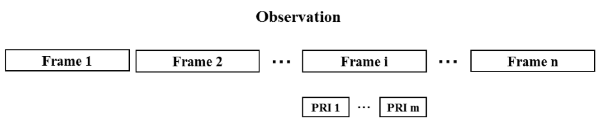

Fig. 1 Sequence of Frames in a typical observation of Mars, a frame being a set of Pulse Repetition Intervals (PRIs)

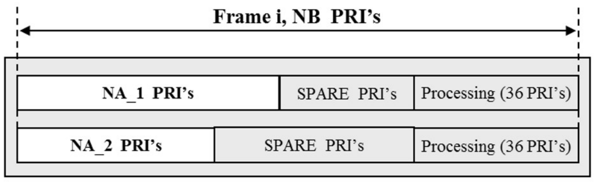

Fig. 2 Internal structure of a generic MARSIS frame

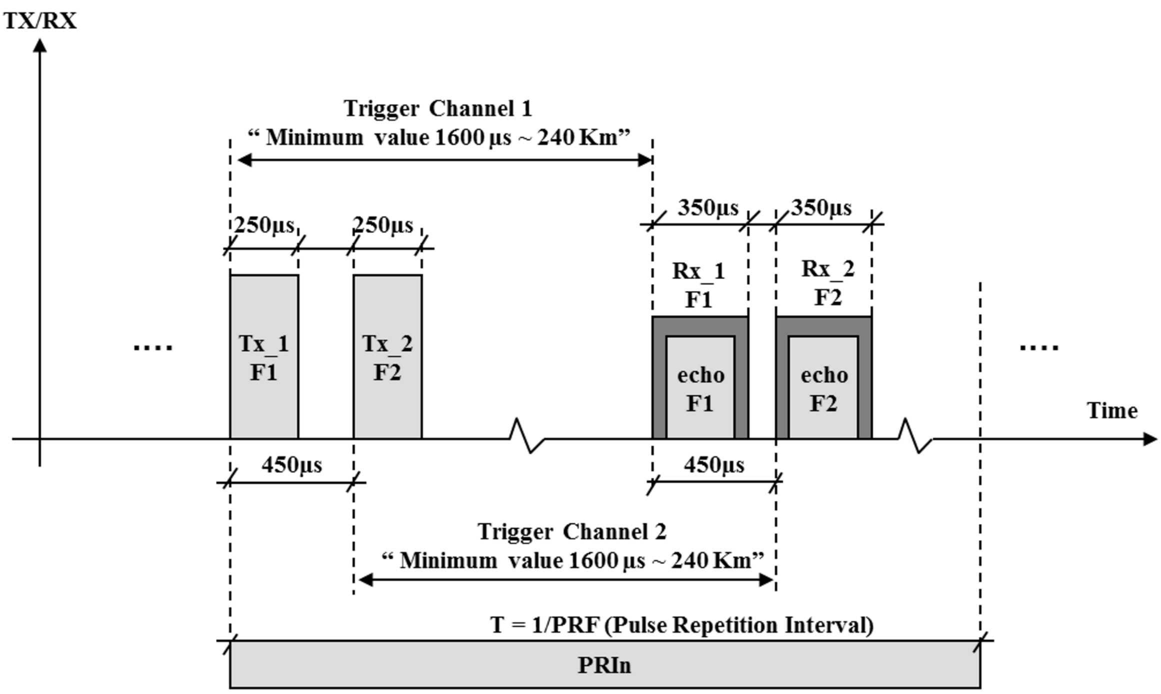

Fig. 3 Single PRI operation, repeated NA times. It includes signal transmission and echo reception.

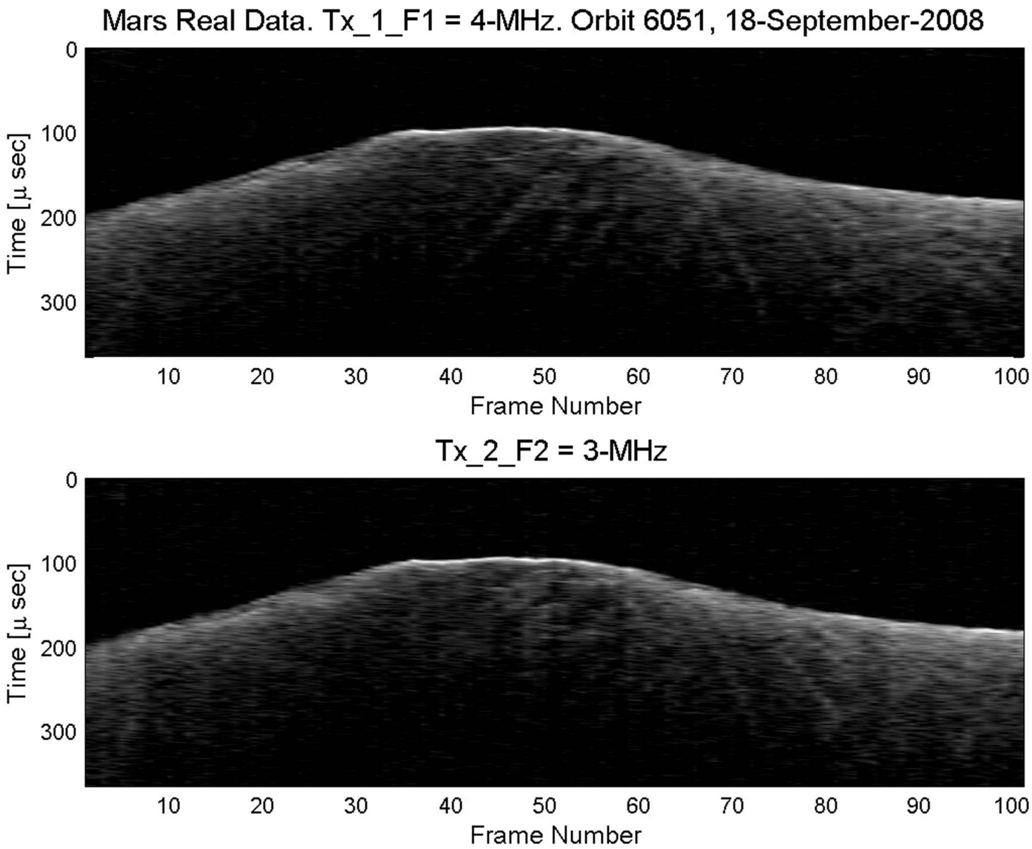

Fig. 4 MARSIS typical acquisition data from orbit 6051, showing a typical observation over Olympus Mons.

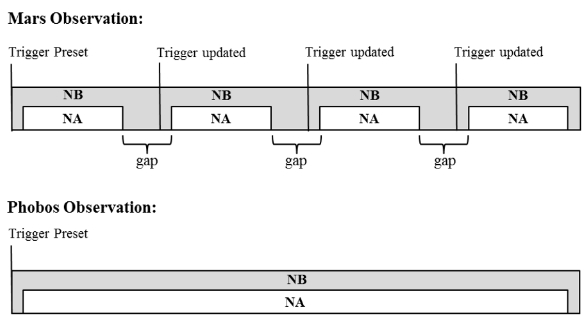

Fig. 5 Top panel shows frames separated by gaps to achieve the best performance on Mars. Bottom panel shows a single synthetic aperture ("Super Frame") more appropriate for the observation and science analysis of Phobos.

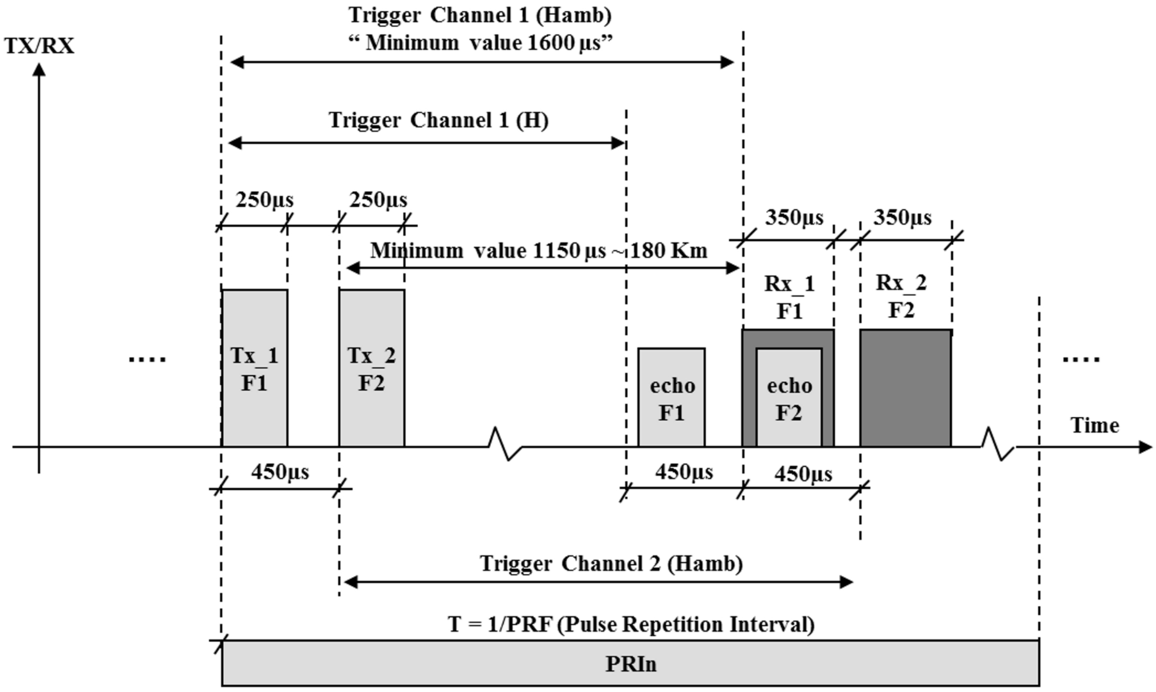

Fig. 6 Scheme of acquisition with the "Range Ambiguity Technique". The instrument is forced to receive the echo of the second transmitted pulse ("echo F2") into the first receiving window (Rx_1_F1). The echo of the first transmitted pulse ("echo F1") is therefore lost and the second receiving window (Rx_2_F2) will sample just cosmic noise.

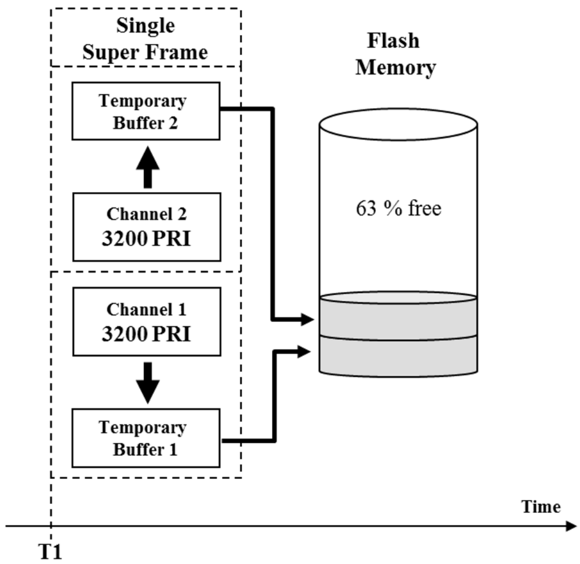

Fig. 7 Acquisition architecture of single super frame, centered on closest approach. This is typically used when the closest approach altitude is higher than 180 km.

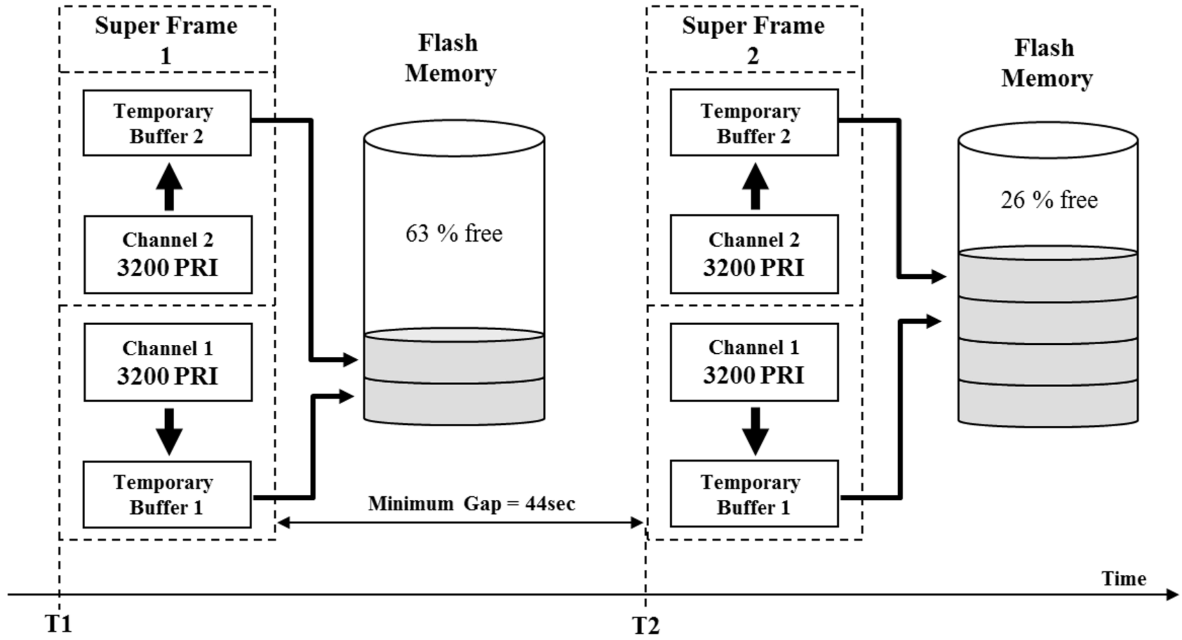

Fig. 8 Acquisition architecture of two super frames symmetric with respect to pericenter. This is typically used when the closest approach altitude is lower than 180 km and the spacecraft is at an altitude lower than 180 km for more than 25 seconds.

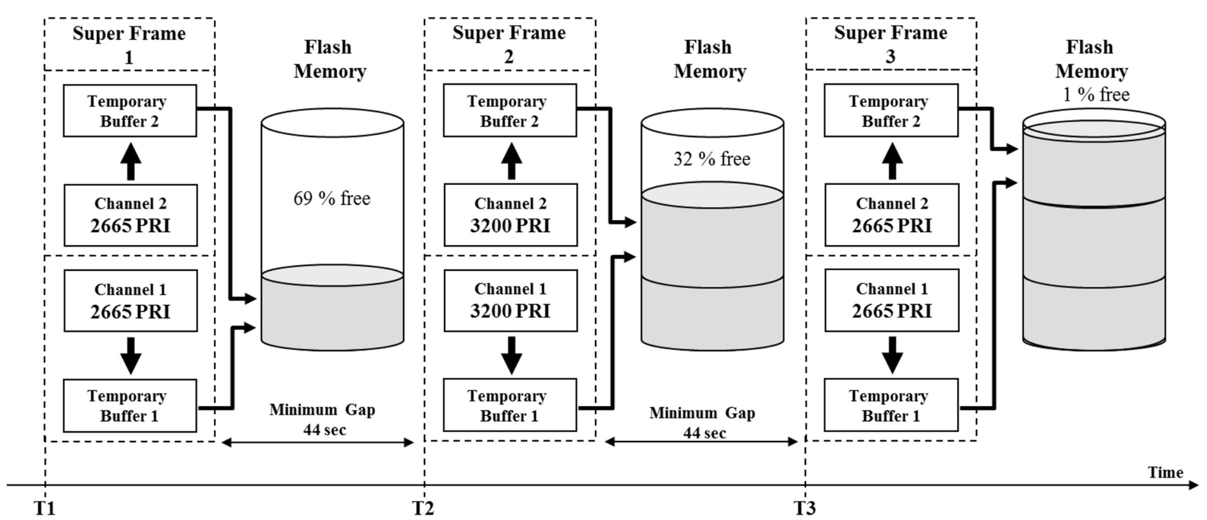

Fig. 9 Acquisition architecture of three super frames, centered on closest approach. This is typically used when the closest approach altitude is higher than 180 km and the space craft altitude, within the first and third super frame is below 350 km.

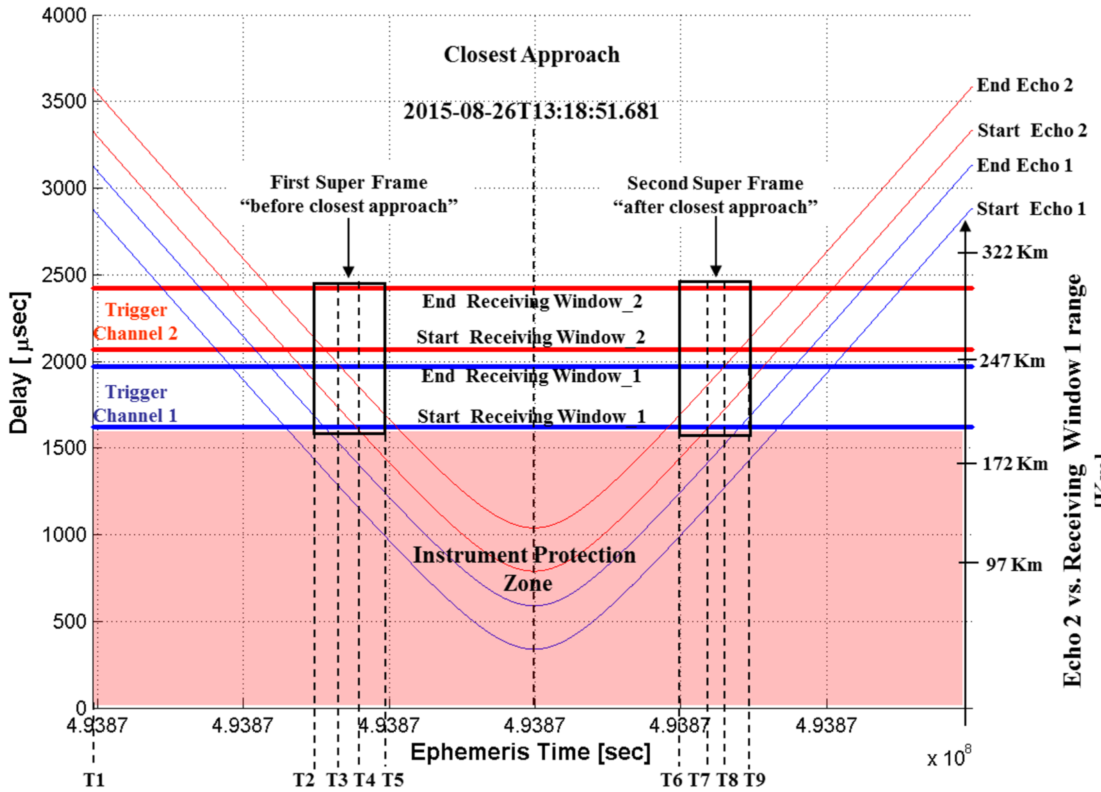

Fig. 10 Simulation over about 4.5 minutes around closest approach. The red area represents the instrument protection zone. The thin blue and red curves represent the ideal receiving windows boundaries for acquiring the two echoes reflected by Phobos' surface from the two chirp waves transmitted by the radar. These ideal values vary following the Phobos range profile. The marked blue and red lines represent the real boundaries programmed for receiving the two echoes.

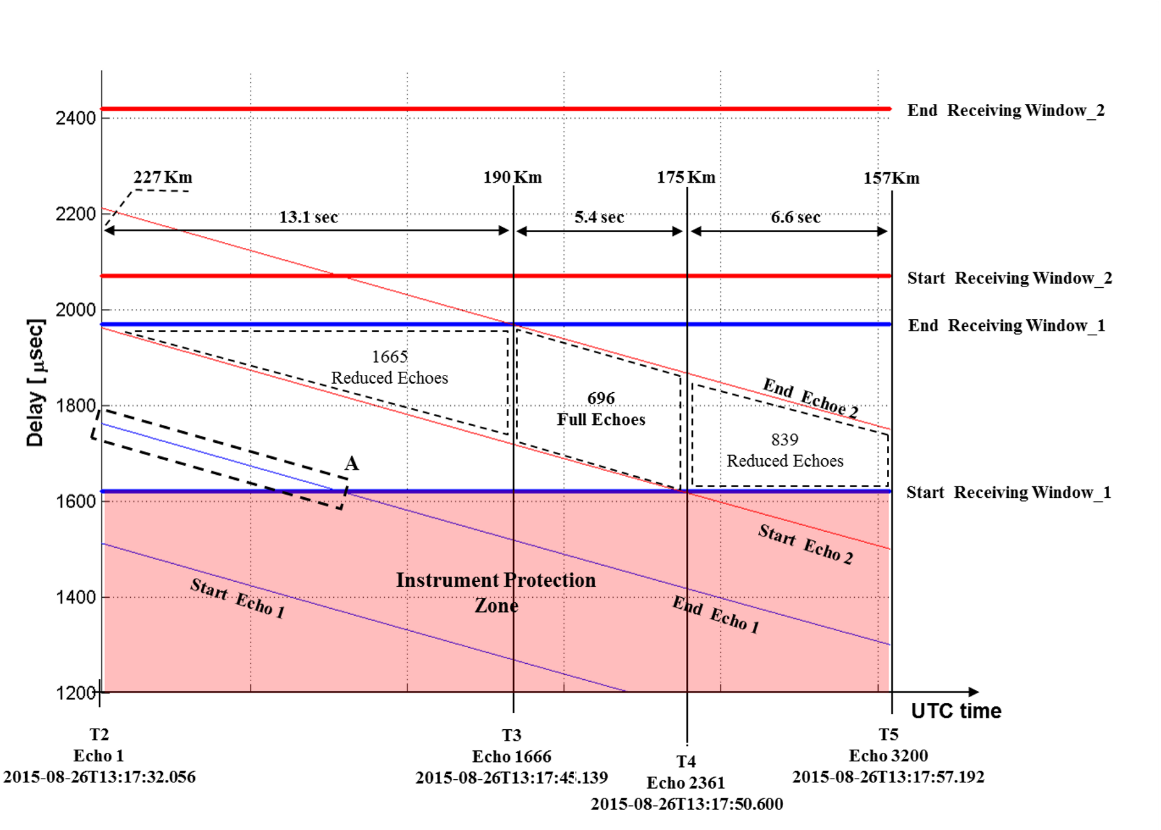

Fig. 11 Approach Super Frame, actual signal distribution. Due to some inaccuracy of the predicted orbital parameters, we obtained a slightly different distribution of the data.

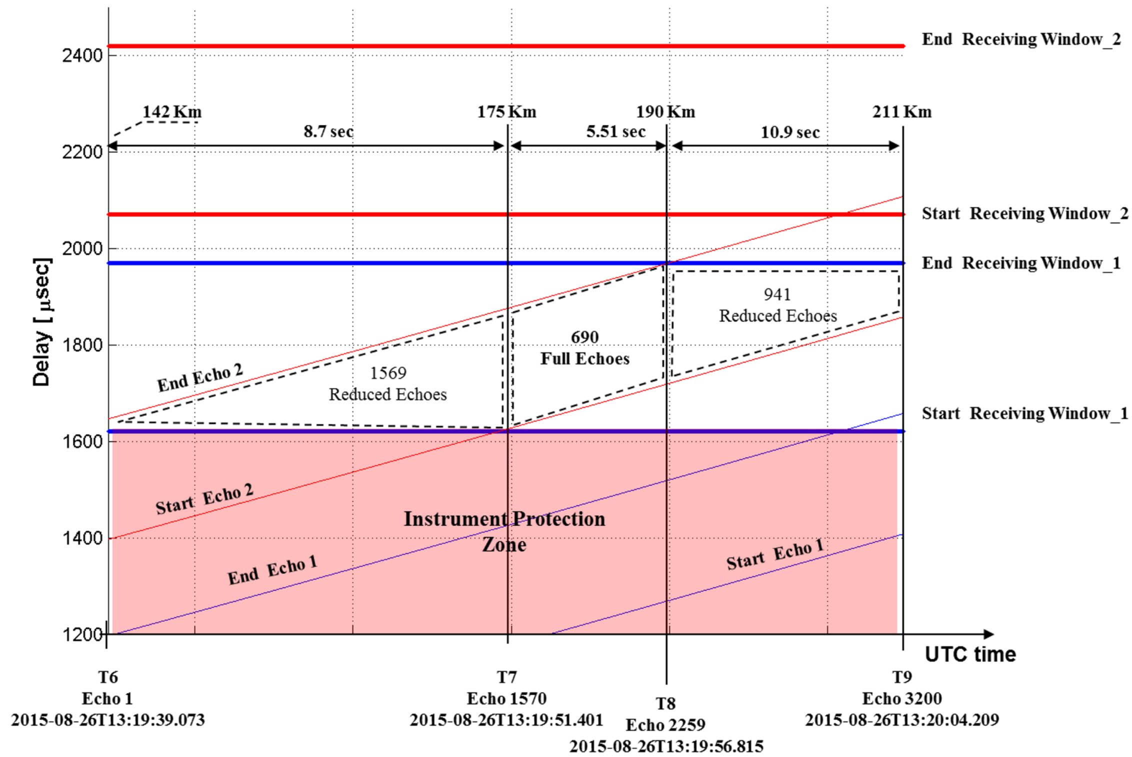

Fig. 12 Departure Super Frame, actual signal distribution. Due to some inaccuracy of the predicted orbital parameters we obtained a slightly different distribution of the data

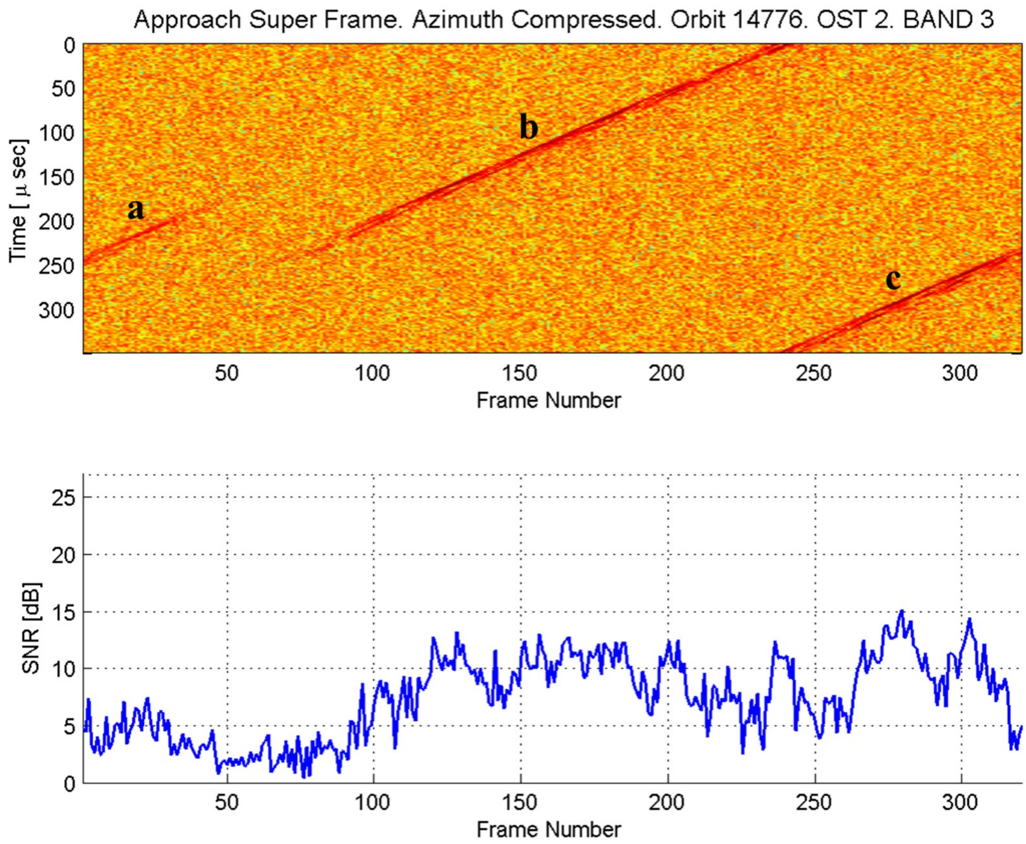

Fig. 13 Phobos science results of the approach super frame. The top panel shows the range and azimuth compression processing. The bottom panel shows the signal to noise ratio(SNR) behavior. The traces "a", "b" and "c" represent the echoes reflected by the Phobos surface.

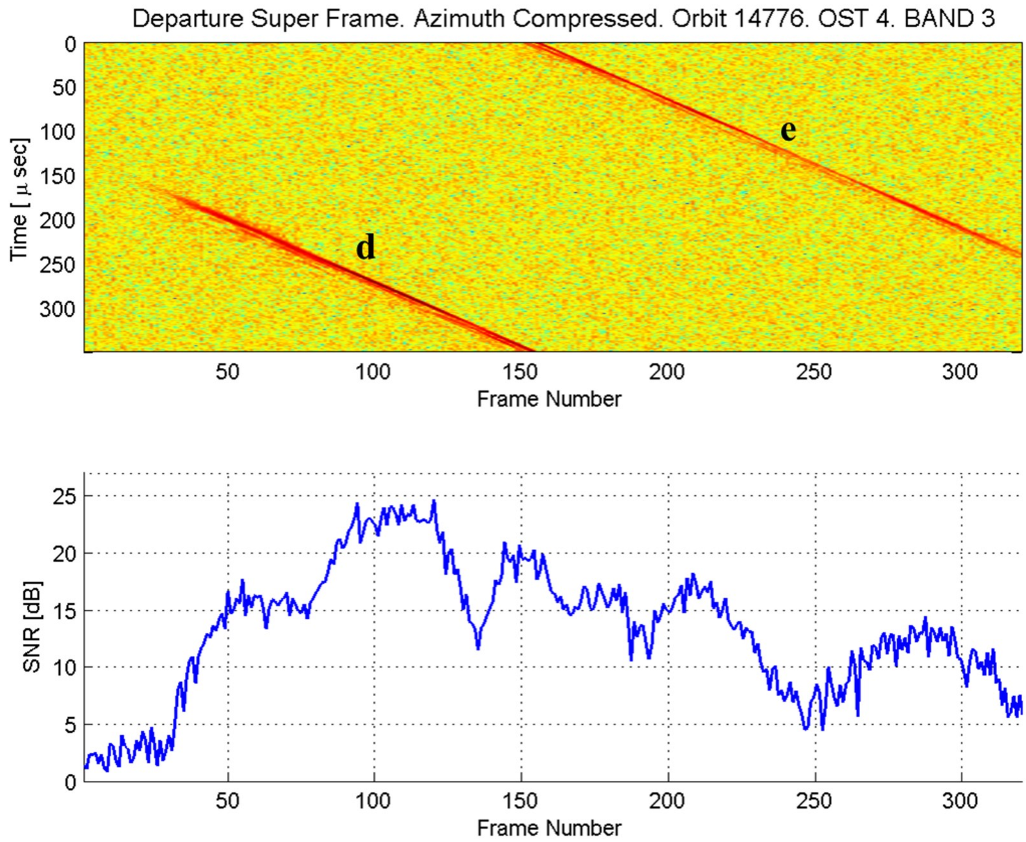

Fig. 14 Phobos science results of the departure super frame. The top panel shows the range and azimuth compression processing. The bottom panel shows the signal to noise ratio (SNR) behavior. The traces "d" and "e" represent the echoes reflected by the Phobos surface.

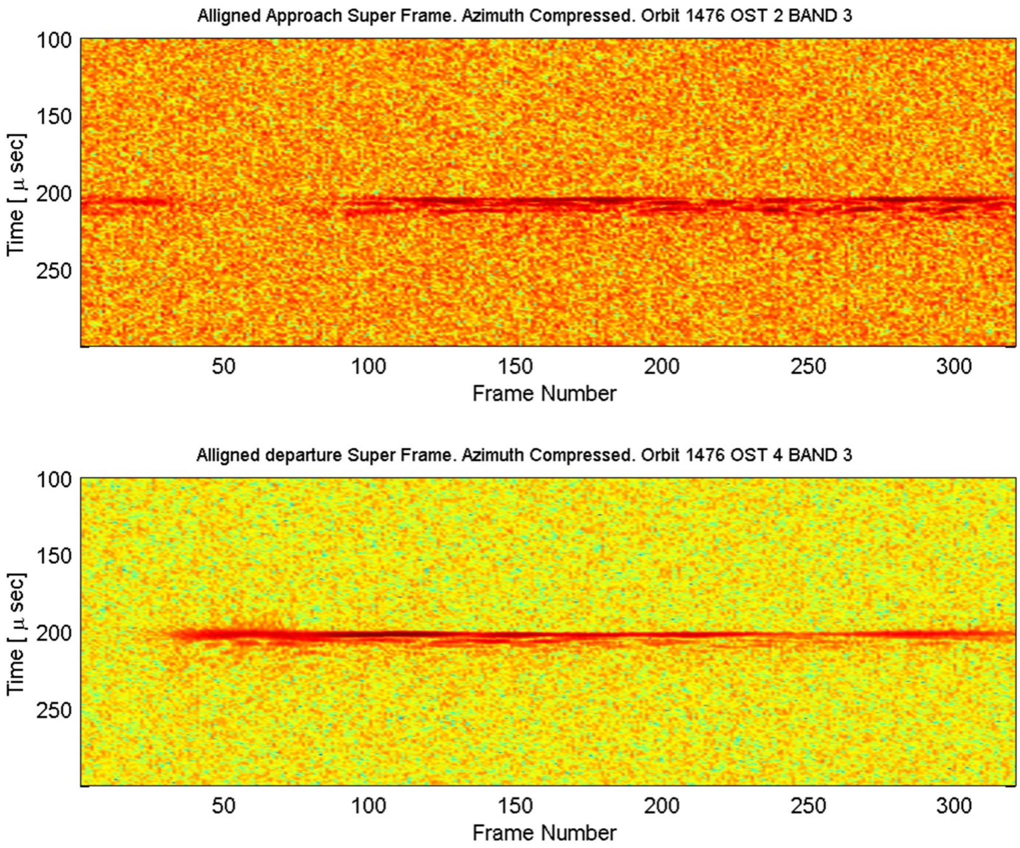

Fig. 15 Phobos radargram of orbit 1476 re aligned with the surface topography. The top panel shows the approach super frame, while the bottom panel shows the departure super frame.

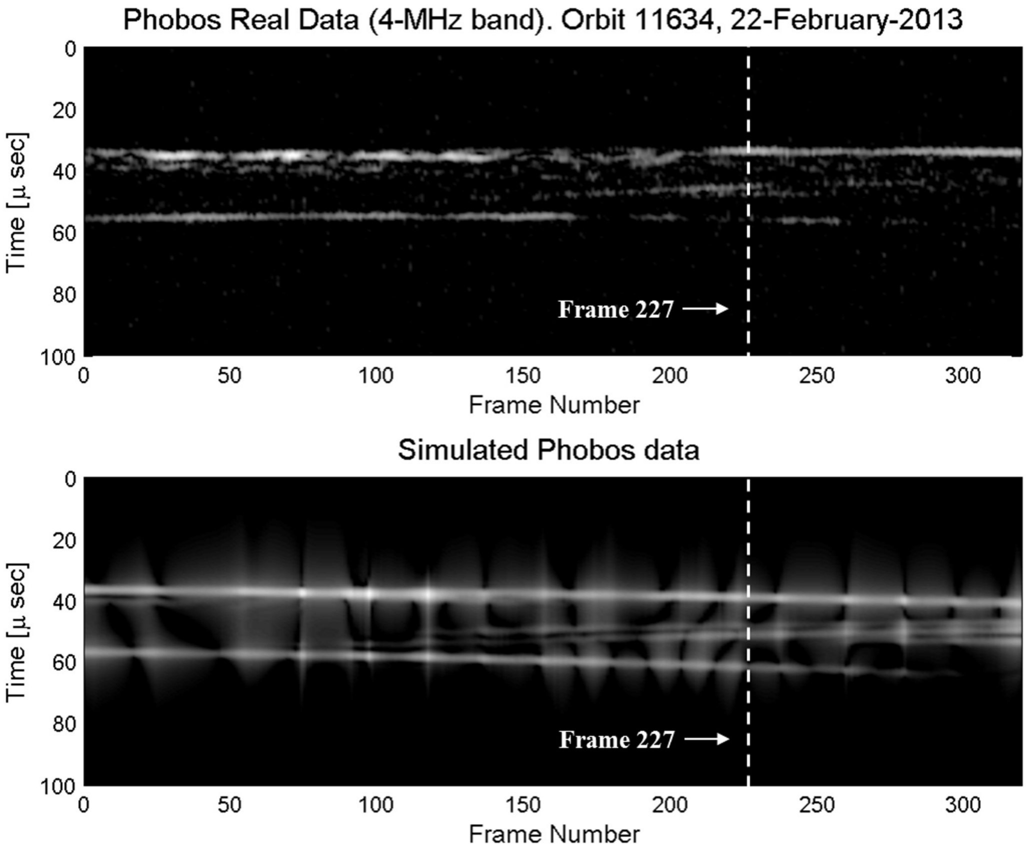

Fig. 16 Phobos radargram of the closest Super Frame. The top panel shows the range and azimuth compression processing of the real data, while the lower panel shows the incoherent simulation of the radar surface returns

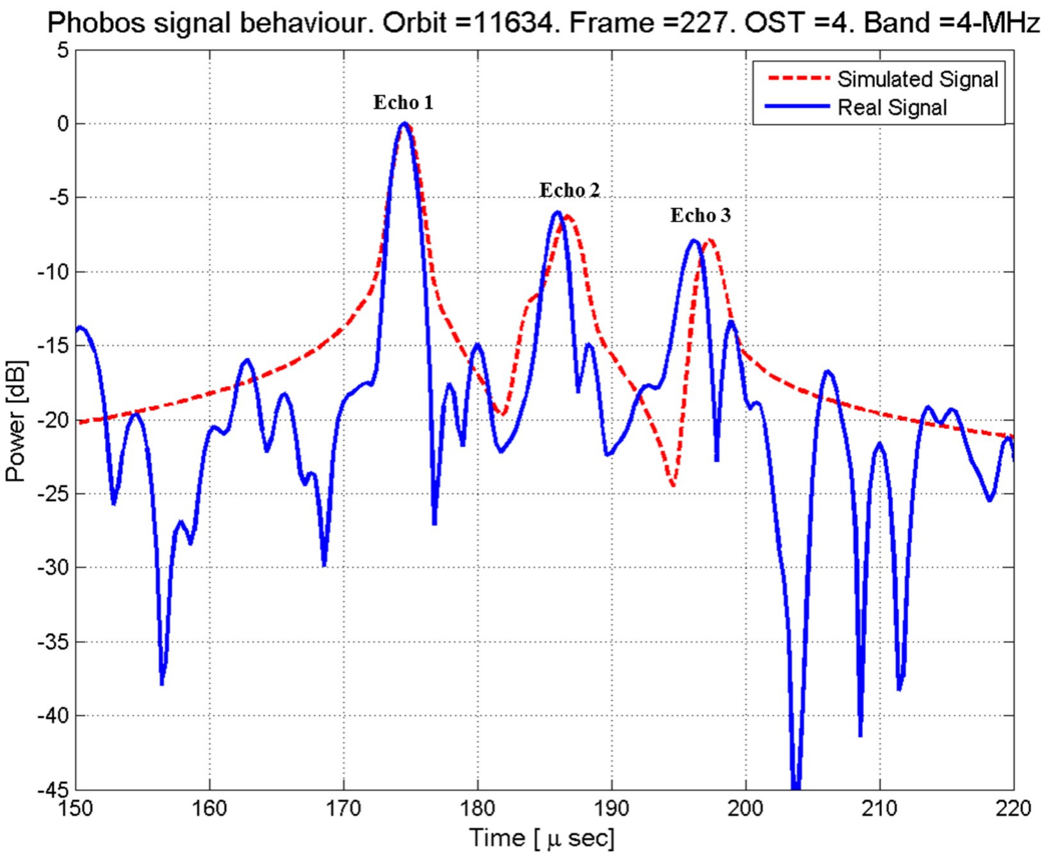

Fig. 17 Frame 227 behavior. The continuous line represents the actual processed data while the dotted line represents the simulated data.